

A degenerate reaction-diffusion SIR model in interconnected regions

Omar Elamraoui* Jawad Salhi † Abderrahim Zafrar ‡

Abstract

This paper presents a novel time-space SIR (Susceptible–Infected–Recovered) model for simulating infectious disease dynamics in two interconnected regions. The model is formulated as a coupled reaction-diffusion system with boundary conditions that dynamically switch from Robin to Neumann types, effectively modelling policy-driven interventions such as lockdowns. A key innovation lies in the incorporation of degenerate diffusion, arising from vanishing population density, which significantly influences transmission behaviour near regional borders. The well-posedness of the model is rigorously established using the Faedo–Galerkin method, ensuring the existence, uniqueness, and positivity of weak solutions. Numerical simulations, performed using the Finite Volume Method, validate the theoretical findings and demonstrate the impact of migration and mobility restrictions on epidemic progression. This framework offers valuable insights for understanding and controlling disease spread in spatially heterogeneous and interconnected settings.

Key words: SIR model, migration dynamics, reaction-diffusion equations, semi-linear degenerate system, Finite Volume Method.

1 Introduction

Mathematical modelling has become an indispensable tool for understanding, predicting, and controlling the spread of infectious diseases. Among the earliest and

*Laboratoire MISI, FST Settât, Univ. Hassan I, 26000 Settât, Morocco (oelamraoui34@gmail.com)

†MAMCS Group, FST Errachidia, Moulay Ismail University of Meknes, Morocco (j.salhi@umi.ac.ma)

‡Department of Mathematics, Faculty of Sciences Dhar El Mahraz, Sidi Mohamed Ben Abdellah University, Fez, Morocco (zafrar.abd@gmail.com)

most influential frameworks are compartmental models, particularly the classical SIR model proposed by Kermack and McKendrick [1]. This model divides the population into three compartments, usually denoted by S (density of susceptible individuals), I (density of infected individuals) and R (density of recovered (or removed) individuals). In its simplest form, the SIR model is described by a system of ordinary differential equations (ODEs). Thanks to its analytical tractability and interpretability, it has been widely used to study various epidemics, including measles, influenza, and COVID-19. However, real-world epidemics involve complex mechanisms that classical ODE-based models cannot fully capture. These mechanisms include spatial heterogeneity, where disease prevalence varies across locations; population mobility and migration, which connect geographically separated regions; and policy-driven interventions, such as vaccination, quarantine, and lockdown measures.

To address these complexities, researchers have developed a wide range of mathematical models, many of which extend the traditional SIR framework. Examples include the Lotka-Volterra model for predator-prey dynamics [2, 3], fractional time-delay epidemic models [4, 5], and various stochastic epidemic models [6, 7, 8, 9]. These approaches, often formulated as partial differential equations (PDEs), make it possible to analyze the spatio-temporal dynamics of host populations and disease propagation, offering a richer description than ODE-based models [10, 11, 12, 13, 14].

While a substantial portion of the existing literature addresses SIR epidemic models for non-degenerate partial differential equations, the mathematical study of these models with degenerate equations remains largely unaddressed. This class of equations presents a unique set of challenging mathematical problems due to the loss of uniform ellipticity in the operators, a phenomenon that can occur either on parts of the boundary or within a subregion of the spatial domain. The operators typically involve variable diffusion coefficients that are not uniformly elliptic over the entire domain, even if they remain so on compact subsets at a positive distance from the degeneracy points. Consequently, the analysis of these systems introduces significant analytical difficulties, particularly regarding the well-posedness of the associated evolution equations. In such contexts, classical tools are often insufficient, necessitating the development of an alternative functional framework, such as weighted Sobolev spaces, which differs from the usual setting for classical PDEs.

Human migration represents another critical factor in epidemic dynamics. It shapes cultural, demographic, and economic landscapes across the globe and significantly influences disease transmission. With globalization, international migration exceeded 281 million people worldwide in 2020 [15]. As a result, many epidemic models have incorporated the effects of migration and immigration [16, 17].

In particular, various SIR-based models accounting for infected immigration were studied by the authors in [16]. The authors in [18] extended this by analyzing models with exposed individuals entering the population, while in [19], the authors developed an SEI model that considers immigration across all compartments. Furthermore, the authors in [20] explored the relationship between disease dynamics and the birthplace of migrant workers.

Despite these contributions, most existing epidemic models assume constant mobility rates and neglect the impact of policy-driven mobility restrictions, such as lockdowns, which have become central to epidemic control strategies. These limitations motivate the development of more realistic frameworks incorporating spatial heterogeneity, migration and degenerate diffusion. In this work, we propose a novel time-space SIR model for two interconnected regions sharing a common interface. Our main contributions are summarized as follows:

1. **Degenerate reaction-diffusion framework:** We formulate the epidemic dynamics as a coupled system of nonlinear reaction-diffusion partial differential equations with boundary degeneracy [21, 22, 23, 24] (PDEs). Degeneracy naturally arises in areas where the population density vanishes, leading to spatial zones with zero mobility (like quarantine, geographic or political barriers).
2. **Migration-dependent boundary dynamics:** Cross-border population movement between the two regions is modelled through nonlinear Robin boundary conditions. When the number of infected individuals exceeds a certain threshold, mobility restrictions are enforced by switching to Neumann boundary conditions to effectively simulate lockdown policies. This component of the model extends our earlier work in [25], where migration effects were considered in a simpler setting without degenerate diffusion.
3. **Well-posedness and numerical analysis:** We prove the existence, uniqueness, and positivity of weak solutions using the Faedo–Galerkin method. The theoretical results are validated through high-resolution numerical simulations based on the Finite Volume Method (FVM).

This modelling framework provides deeper insights into the interplay between migration, degenerate diffusion, and policy-driven mobility restrictions, offering a more realistic representation of epidemic dynamics in interconnected regions.

The remainder of this paper is structured as follows: In Section 2, we present our time-space SIR model, which is formulated as a reaction-diffusion system with mixed boundary conditions. In Section 3, we demonstrate the model’s well-posedness utilizing the Faedo–Galerkin method. Finally, Section 4 introduces the finite volume method that will be employed in Section 5 for numerical examples and simulations to validate and illustrate our results.

2 Formulation of a degenerate reaction-diffusion SIR model incorporating immigration

For a time horizon $T > 0$, let $\Omega \subset \mathbb{R}^d$ (where $d \in \{1, 2\}$) be a domain decomposed into two contiguous subregions, Ω_1 and Ω_2 , such that $\Omega = \Omega_1 \cup \Omega_2$. The external (unshared) boundary of each subregion is denoted by $\partial\Omega_i$ for $i \in \{1, 2\}$, while $\Gamma := \partial\Omega_1 \cap \partial\Omega_2$ represents their shared "virtual" interface.

This section is devoted to the development of a model for studying immigration dynamics between the regions of Ω across the common interface Γ , while incorporating relevant policy considerations. First, we introduce our main assumption and provide its formal mathematical justification.

- *Main assumption:*

For $i, j \in \{1, 2\}$ with $i \neq j$, we assume that each individual in $\bar{\Omega}_j$ has a probability $\lambda_j(\cdot, \cdot) : [0, T] \times \bar{\Omega}_i \mapsto [0, 1]$ of being in $\bar{\Omega}_i$. This means that we are concerned with the new location of the individual in Ω_i , regardless of its previous location in $\bar{\Omega}_j$. Also, this accounts for the immigration of individuals into $\bar{\Omega}_i$ before the disease is detected in that region. Consequently, on one side, we must assume that diffusion occurs for both residents (individuals originally in Ω_i) and immigrants (individuals from Ω_j). On the other side, the probability λ_j is defined such that $\lambda_j(t, x) = 0$ for all $(t, x) \in [0, T] \times \partial\Omega_i$ (i.e., at the unshared boundaries of Ω_i and outside Ω), and it maybe used to measure the number of individuals in units of measure (for example using the Poisson process [26]). Conversely, for all $(t, x) \in [0, T] \times \Omega_i$, we have $\lambda_j(t, x) > 0$. Similarly, we assume that each resident in Ω_i has a probability λ_i of leaving the region before disease detection is made. Furthermore, the diffusion in region i is directly dependent on this probability $\lambda_i \in [0, 1]$. Thus, if $\lambda_i = 0$, the diffusion coefficient $\sigma_i(t, x, \lambda_i) := \kappa(t)D(x, \lambda_i)$ vanishes, leading to a degenerate reaction-diffusion system of coupled partial differential equations.

$\lambda_j > 0$ indicates that individuals originating from Ω_j (including susceptible, infected, and recovered classes) are present within Ω_i . Specifically, infected immigrants from Ω_j can introduce new sources of infection. Consequently, susceptible individuals in Ω_i are subject to infection from two pathways: from local infectious individuals within Ω_i at rate β_i , and from immigrants from Ω_j at rate β_{ij} .

Now, we define the notations used throughout the paper:

- β_i is the infection rate in the domain Ω_i .
- β_{ij} is the infection rate between two individuals of Ω_i and Ω_j .
- γ_i is the recovery rate in the domain Ω_i .

- $\lambda_{.,j}$ (resp. $\lambda_{.,i}$) is the probability of being in Ω_i from Ω_j (resp. in Ω_j from Ω_i).
- α^i is the migration and immigration rate of individuals across Γ .
- Λ_i is the birth rate in each sub-domain Ω_i .
- μ_S, μ_I and μ_R are the natural death rates for each compartment.
- N_i is the total population in the domain Ω_i .

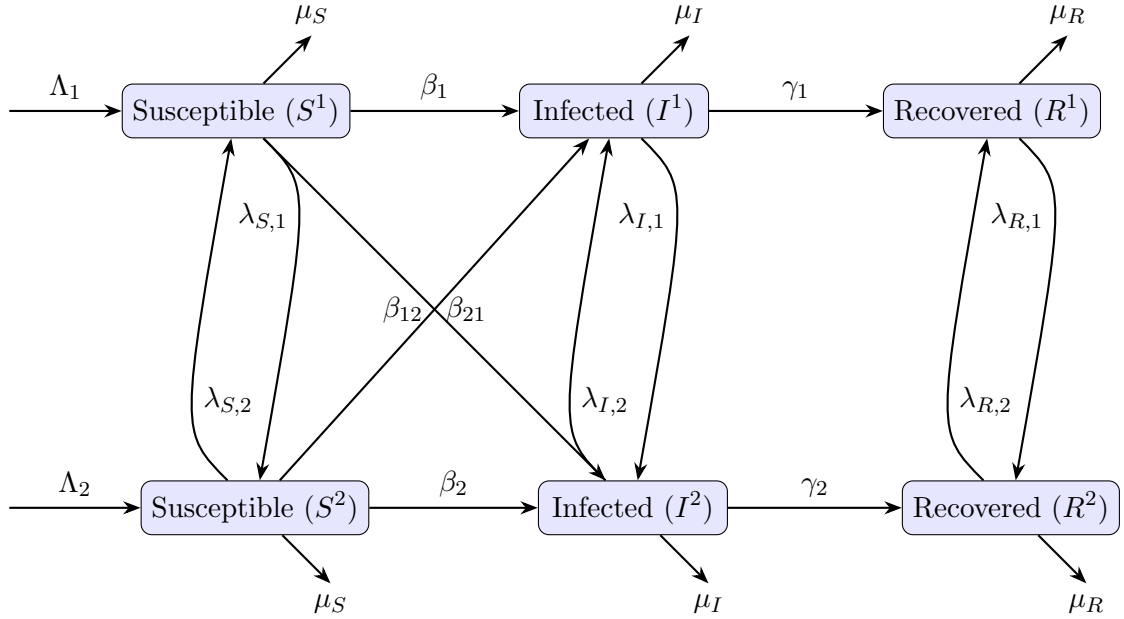


Figure 1: SIR model with cross-transitions, birth, and death rates.

Considering the assumptions mentioned above, we investigate their influence on the evolution of individuals within domains Ω_i for $i \in \{1, 2\}$. This leads to the following model, defined for $i, j \in \{1, 2\}$, $i \neq j$ and $Q_i := (0, T) \times \Omega_i$:

$$\begin{cases} \partial_t S^i - \operatorname{div}(\sigma(\lambda_S) \cdot \nabla S) = \Lambda_i N_i - (\beta_i I^i + \beta_{ij} I^j) S^i + \lambda_{S,j} S^j - (\lambda_{S,i} + \mu_S) S^i, & \text{in } Q_i \\ \partial_t I^i - \operatorname{div}(\sigma(\lambda_I) \cdot \nabla I) = (\beta_i I^i + \beta_{ij} I^j) S^i - \gamma_i I^i + \lambda_{I,j} I^j - (\lambda_{I,i} + \mu_I) I^i, & \text{in } Q_i \\ \partial_t R^i - \operatorname{div}(\sigma(\lambda_R) \cdot \nabla R) = \gamma_i I^i + \lambda_{R,j} R^j - (\lambda_{R,i} + \mu_R) R^i & \text{in } Q_i \end{cases} \quad (1)$$

where $\sigma(\lambda_k) := (\sigma_i(\lambda_{k,i}), \sigma_j(\lambda_{k,j}))$ for $i \in \{1, 2\}$ and $k \in \{S, I, R\}$. Moreover, we denoted $\nabla S^\top := (\nabla S^i, \nabla S^j)^\top$ and $v \cdot w$ is the inner product.

The problem (1) will be associated with the Dirichlet boundary conditions:

$$S^i = I^i = R^i = 0, \quad \text{on } [0, T] \times \partial\Omega_i, \text{ for } i \in \{1, 2\}, \quad (2)$$

and the following initial conditions:

$$\begin{cases} S^i(0, x) = S_0(x, \lambda_{S,i}, \lambda_{S,j}) \geq 0, \\ I^i(0, x) = I_0(x, \lambda_{I,i}, \lambda_{I,j}) \geq 0, \\ R^i(0, x) = R_0(x, \lambda_{R,i}, \lambda_{R,j}) \geq 0, \end{cases} \quad (3)$$

meaning that the initial number of individuals in the considered region Ω_i depends on the probability of leaving or being in this region. So, essentially, we are dealing with a semi-linear boundary weakly degenerating parabolic problem.

We assume the following constraint on the virtual interface Γ :

$$\begin{cases} \sigma(\lambda_S) \cdot \nabla S \cdot \tau_i + \alpha_S^j(I^i) S^j = 0 \\ \sigma(\lambda_I) \cdot \nabla I \cdot \tau_i + \alpha_I^j(I^i) I^j = 0 \\ \sigma(\lambda_R) \cdot \nabla R \cdot \tau_i + \alpha_R^j(I^i) R^j = 0 \end{cases} \quad \text{on } [0, T] \times \Gamma. \quad (4)$$

The notation τ_i (respectively η_i) stands for outward boundary normal vectors from Ω_i on the boundary Γ (respectively $\partial\Omega_i$). For simplicity of the notation, let us set $\tau = \tau_1 = -\tau_2$.

The function $\alpha_k^j(I)$ models the direction of the movement between two regions and is defined for $k \in \{S, I, R\}$ as follows:

$$\alpha_k^j(I) := \begin{cases} \alpha(I), & \text{if } I \geq I_{\text{th}}^j, \\ -\alpha(I), & \text{otherwise,} \end{cases}$$

where I_{th}^j is a threshold value specific to the region Ω_j .

We suppose $\alpha(\cdot)$ to be a Lipschitz continuous function such that

$$\alpha(n) \rightarrow 0 \quad \text{as } n \rightarrow +\infty.$$

Here are a few typical examples that can be considered is:

$$\alpha(I) = \frac{1}{1 + I^2}, \quad \alpha(I) = e^{-I}.$$

In real-world applications, $\alpha(I)$ represents the mobility or transfer rate of individuals between regions, and it decreases as the number of infected individuals increases. This reflects the realistic assumption that higher infection levels reduce movement

due to health precautions or public policies.

When the number of infected individuals in region Ω_j exceeds the threshold I_{th}^j , individuals are assumed to leave region Ω_i and move toward Ω_j , with mobility rate $\alpha(I)$. Conversely, if the infection level in Ω_j is below the threshold, individuals may migrate in the opposite direction, from Ω_j to Ω_i , with mobility rate $-\alpha(I)$.

In extreme cases, such as during a pandemic, a lockdown policy may be enforced, corresponding to $\alpha(I) = 0$. This scenario models a complete halt of mobility between regions. The condition $\alpha(I) \rightarrow 0$ as $I \rightarrow +\infty$ captures this behavior, reflecting that as infection levels become very large, mobility naturally tends to zero due to restrictive public health measures.

Remark 1. *The nonlinear virtual interface conditions (4) are prescribed on the interface between two subregions of Ω . They not only serve to model the lockdown but also act as coupling constraints, ensuring the correct transmission of information across the subdomains of Ω .*

In the next section, we aim to prove the well-posedness of the problem stated above. For this purpose, we will need the following assumptions:

$$\begin{aligned} \sigma_i &\in C^0(\overline{Q_i}) \cap C^1(Q_i) \text{ and is positive in } [0, T] \times \Omega_i, \\ \frac{\partial_t \sigma_i}{\sigma_i} &\in L^\infty(Q_i). \end{aligned}$$

and there exists $0 < \delta < \min\{t, T - t\}$ such that

$$\int_{t-\delta}^{t+\delta} \int_{\Omega_i \cap B_\delta(x)} \frac{1}{\sigma_i(\lambda_i(y, s))} dy ds < +\infty \quad \forall t \in (0, T), \quad (5)$$

with $B_\delta(x)$ being the ball in \mathbb{R}^d centered at x and with radius δ . Consequently, our analysis will focus on the case of weak degeneracy (see [27]).

3 Well-posedness of the problem

In this section, we prove the well-posedness of the initial boundary value problem (1)-(3). To this end, we introduce the following notations

$$u^i = \begin{pmatrix} S^i \\ I^i \\ R^i \end{pmatrix}, \quad \nabla u^i = \begin{pmatrix} \nabla S^i \\ \nabla I^i \\ \nabla R^i \end{pmatrix},$$

$$f(u^i, u^j) = \begin{pmatrix} \Lambda_i N_i - \mu_S S^i - (\beta_i I^i + \beta_{ij} I^j) S^i \\ (\beta_i I^i + \beta_{ij} I^j) S^i - (\gamma_i + \mu_I) I^i \\ \gamma_i I^i - \mu_R R^i \end{pmatrix}, \quad \lambda_i = \begin{pmatrix} \lambda_{S,i} \\ \lambda_{I,i} \\ \lambda_{R,i} \end{pmatrix},$$

$A_i(\lambda_i) := \text{diag}(\sigma_{S,i}, \sigma_{I,i}, \sigma_{R,i})$, where $\sigma_{\cdot,i} = \sigma_i(\lambda_{\cdot,i})$, and $\alpha^j = \text{diag}(\alpha_S^j(I^i), \alpha_I^j(I^i), \alpha_R^j(I^i))$.
Then the problem (1)-(3) becomes:

$$\begin{cases} \partial_t u^i - \text{div}(A_i(\lambda_i) \nabla u^i) = f(u^i, u^j) + \text{div}(A_j(\lambda_j) \nabla u^j) + \lambda_j u^j - \lambda_i u^i, & \text{in } Q_i \\ A_i(\lambda_i) \nabla u^i \cdot \tau + A_j(\lambda_j) \nabla u^j \cdot \tau + \alpha^j(I^i) u^j = \mathbf{0}, & \text{on } [0, T] \times \Gamma \\ u^i = \mathbf{0} & \text{on } [0, T] \times \partial\Omega_i \\ u^i(0, x) = u_0^i(x, \lambda_i, \lambda_j) & \text{in } \Omega_i \\ \text{for all } i, j = 1, 2 \text{ and } i \neq j. \end{cases} \quad (6)$$

Before going further, let us first introduce some weighted Sobolev spaces that are naturally associated with degenerate operators:

$$\mathbf{H}_{A_i}^1(\Omega) := \left\{ u \in \mathbf{L}^2(\Omega) := L^2(\Omega)^3 : \nabla u \cdot A_i \nabla u \in \mathbf{L}^1(\Omega) := L^1(\Omega)^3 \right\}$$

endowed with the norm

$$\|u\|_{\mathbf{H}_{A_i}^1}^2 := \int_{\Omega} |u|^2 + \int_{\Omega} |A_i^{\frac{1}{2}} \nabla u|^2, \quad \forall u \in \mathbf{H}_{A_i}^1(\Omega).$$

It is easy to observe that the classical Sobolev space $\mathbf{H}^1(\Omega) \subset \mathbf{H}_{A_i}^1(\Omega)$. We also denote

$$\mathbf{H}_{A_i}^2(\Omega) = \left\{ u \in \mathbf{H}_{A_i}^1(\Omega) : \text{div}(A_i \nabla u) \in \mathbf{L}^2(\Omega) \right\}$$

with the associated norm defined by

$$\begin{aligned} \|u\|_{\mathbf{H}_{A_i}^2}^2 &:= \|u\|_{\mathbf{H}_{A_i}^1}^2 + \|\text{div}(A_i \nabla u)\|_{\mathbf{L}^2}^2 \\ &= \int_{\Omega_i} |u|^2 + \int_{\Omega} |A_i^{\frac{1}{2}} \nabla u|^2 + \int_{\Omega} |\text{div}(A_i \nabla u)|^2, \quad \forall u \in \mathbf{H}_{A_i}^2(\Omega). \end{aligned}$$

Remark 2. *It is worth noting that, for these natural norms, $\mathbf{H}_{A_i}^1(\Omega)$, $\mathbf{H}_{A_i}^2(\Omega)$ are Hilbert spaces. Moreover, we have the following continuous embeddings are satisfied*

$$\mathbf{H}^1(\Omega) \hookrightarrow \mathbf{H}_{A_i}^1(\Omega) \hookrightarrow \mathbf{L}^2(\Omega); \quad \mathbf{H}_{A_i}^2(\Omega) \hookrightarrow \mathbf{H}_{A_i}^1(\Omega).$$

Additionally, we have that $\mathbf{H}_{A_i}^1(\Omega) \subset \mathbf{H}_{loc}^1(\Omega)$ and $\mathbf{H}_{A_i}^2(\Omega) \subset \mathbf{H}_{loc}^2(\Omega)$.

In view of [28, Lemma 1], we have $C^\infty(\overline{\Omega})$ is dense in $\mathbf{H}_{A_i}^1(\Omega)$. This permits to define

$$\mathbf{H}_{A_i,0}^1(\Omega_i) := \overline{\{u \in C^\infty(\overline{\Omega}) \mid \text{supp}(u) \subset\subset \Omega\}}^{\mathbf{H}_{A_i}^1(\Omega)}.$$

Furthermore, the space $\mathbf{H}_{A_i,0}^1(\Omega)$ can be endowed with the norm

$$|u|_{A_i,0}^2 := \int_{\Omega} |A_i^{\frac{1}{2}} \nabla u|^2, \quad \forall u \in \mathbf{H}_{A_i,0}^1(\Omega),$$

which is equivalent to the norm $\|\cdot\|_{\mathbf{H}_{A_i,0}^1(\Omega_i)}$ in $\mathbf{H}_{A_i,0}^1(\Omega_i)$.

The following compactness results hold (for the proofs, see [29, Theorem 3.4]):

Proposition 1. *One has*

1. *The space $\mathbf{H}_{A_i,0}^1(\Omega)$ is compactly imbedded in $\mathbf{L}^2(\Omega)$.*

After recalling the definition and key results concerning the weighted Sobolev space, along with some of its important continuity and compact embedding properties known in the literature, we now define the weak solution of the system (6).

Definition 1. *We say that a function $u = (u^1, u^2)$ such that*

$$(u^1, u^2) \in \mathbf{L}^2(0, T; \mathbf{H}_{A_1,0}^1(\Omega)) \times \mathbf{L}^2(0, T; \mathbf{H}_{A_2,0}^1(\Omega))$$

and

$$(\partial_t u^1, \partial_t u^2) \in \mathbf{L}^2(0, T; \mathbf{H}_{A_1,0}^{-1}(\Omega)) \times \mathbf{L}^2(0, T; \mathbf{H}_{A_2,0}^{-1}(\Omega))$$

is a weak solution of the degenerate initial/boundary value problem (6) provided for almost every $t \in (0, T)$ and for all test functions $(v^1, v^2) \in \mathbf{L}^2(0, T; \mathbf{H}_{A_1,0}^1(\Omega)) \times \mathbf{H}_{A_2,0}^1(\Omega)$:

$$\left\{ \begin{array}{l} \int_{\Omega_i} \partial_t u^i v^i + \int_{\Omega_i} A_i(\lambda_i) \nabla u^i \cdot \nabla v^i + \int_{\Omega_i} A_j(\lambda_j) \nabla u^j \cdot \nabla v^i = \int_{\Omega_i} f(u^i, u^j) v^i + \\ \int_{\Gamma} \alpha^j(u^i) u^j v^i \quad + \int_{\Omega_i} \lambda_j u^j v^i - \int_{\Omega_i} \lambda_i u^i v^i, \\ \text{for all } i, j = 1, 2 \text{ and } i \neq j. \end{array} \right. \quad (7)$$

and

$$u^i(0, x) = u_0^i(x) \quad \text{in } \Omega_i, \quad \text{for } i = 1, 2,$$

where $u_0^i \in \mathbf{L}^2(\Omega)$ are given initial data.

Next, we state our main result on the well-posedness of the degenerate problem (6).

Theorem 1. *Let $T > 0$ and $u_0^i \in \mathbf{L}^2(\Omega)$, $i = 1, 2$, then the problem (6) admits a unique non-negative weak solution $(u^1, u^2) \in \mathbf{L}^\infty(0, T, \mathbf{L}^2(\Omega))^2 \cap \mathbf{L}^2(0, T, \mathbf{H}_{A_1,0}^1(\Omega)) \times \mathbf{L}^2(0, T, \mathbf{H}_{A_2,0}^1(\Omega))$ and $(\partial_t u^1, \partial_t u^2) \in \mathbf{L}^2(0, T, \mathbf{H}_{A_1,0}^{-1}(\Omega)) \times \mathbf{L}^2(0, T, \mathbf{H}_{A_2,0}^{-1}(\Omega))$.*

The proof of Theorem 1 relies on the classical Galerkin method and a truncation technique. A first step in this process is establishing the well-posedness of an intermediate problem. Let $g : \mathbf{H}_{A_1}^1(\Omega) \times \mathbf{H}_{A_2}^1(\Omega) \rightarrow \mathbf{L}^2(\Omega)$ be a globally Lipschitz function with a Lipschitz constant $L_g > 0$, satisfying $g(0, 0) = 0$. We consider the following problem

$$\left\{ \begin{array}{ll} \partial_t u^i - \operatorname{div}(A_i(\lambda_i) \nabla u^i) = g(u^i, u^j) + \operatorname{div}(A_j(\lambda_j) \nabla u^j) + \lambda_j u^j - \lambda_i u^i, & \text{in } Q_i \\ A_i(\lambda_i) \nabla u^i \cdot \tau + A_j(\lambda_j) \nabla u^j \cdot \tau + \alpha^j (I^i) u^j = \mathbf{0}, & \text{on } [0, T] \times \Gamma \\ u^i = \mathbf{0} & \text{on } [0, T] \times \partial\Omega_i \\ u^i(0, x) = u_0^i(x, \lambda_i, \lambda_j) & \text{in } \Omega_i \\ \text{for all } i, j = 1, 2 \text{ and } i \neq j. & \end{array} \right. \quad (8)$$

Let us define the auxiliary operator

$$\begin{aligned} \mathcal{I} : L^2(\Omega_1) \times L^2(\Omega_2) &\rightarrow L^2(\Omega_1) \times L^2(\Omega_2), \\ (v_1, v_2) &\mapsto \mathcal{I}(v_1, v_2) = (\lambda_2 v_2, \lambda_1 v_1), \end{aligned} \quad (9)$$

and recall that $\lambda_i \in [0, 1]$ represents the probability that an individual migrates from Ω_i to the other domain. Under the main assumption, \mathcal{I} is well-defined: each individual can immigrate, so that v_i may contribute to Ω_j whenever the probability of immigration from Ω_i to Ω_j is positive, i.e. $\lambda_i > 0$ for $i \neq j$ which in such case means that v_i is well defined on the domain Ω_j by its new location. In addition, it is straightforward to show that this operator is linear and bounded, i.e. $\exists M_{\mathcal{I}} > 0$ such that

$$\|\mathcal{I}(v_1, v_2)\|_{L^2(\Omega_1) \times L^2(\Omega_2)} \leq M_{\mathcal{I}} \|(v_1, v_2)\|_{L^2(\Omega_1) \times L^2(\Omega_2)}. \quad (10)$$

We now establish the well-posedness of the intermediate problem (8).

Proposition 2. *Let $T > 0$ and $u_0^i \in \mathbf{L}^2(\Omega)$, $i = 1, 2$. The problem (8) admits a unique non-negative weak solution $(u^1, u^2) \in \mathbf{L}^\infty(0, T, \mathbf{L}^2(\Omega))^2 \cap \mathbf{L}^2(0, T, \mathbf{H}_{A_1,0}^1(\Omega)) \times \mathbf{L}^2(0, T, \mathbf{H}_{A_2,0}^1(\Omega))$ and $(\partial_t u^1, \partial_t u^2) \in \mathbf{L}^2(0, T, \mathbf{H}_{A_1,0}^{-1}(\Omega)) \times \mathbf{L}^2(0, T, \mathbf{H}_{A_2,0}^{-1}(\Omega))$.*

Proof. The proof is based on the Faedo-Galerkin procedure.

Step 1: Existence in finite dimension

The space $\mathbf{L}^2(\Omega)$ is a separable space, hence there exists an increasing sequence of subspace $\mathbf{V}_n \subset \mathbf{V}_{n+1}$ which are dense in $\mathbf{L}^2(\Omega)$ where for every $n \geq 0$ the finite dimensional space \mathbf{V}_n is defined by

$$\mathbf{V}_n = \text{span} \{v_1, v_2, \dots, v_n\}$$

such that $\{v_1, v_2, \dots, v_n, \dots\}$ is a complete orthonormal basis of $\mathbf{L}^2(\Omega_i)$ i.e., $\|v_i\|_{\mathbf{L}^2(\Omega)} = 1$ and $\langle v_i, v_j \rangle_{\mathbf{L}^2(\Omega_i)} = 0, \forall i \neq j$.

We consider the following finite problem corresponding to (8) on \mathbf{V}_n :

$$\left\{ \begin{array}{ll} \partial_t u_n^i - \text{div}(A_i(\lambda_i) \nabla u_n^i) = g(u_n^i, u_n^j) + \text{div}(A_j(\lambda_j) \nabla u_n^j) + \lambda_j u_n^j - \lambda_i u_n^i, & \text{in } Q_i \\ A_i(\lambda_i) \nabla u_n^i \cdot \tau + A_j(\lambda_j) \nabla u_n^j \cdot \tau + \alpha^j (I^i) u_n^j = \mathbf{0}, & \text{on } [0, T] \times \Gamma \\ u_n^i = \mathbf{0}, & \text{on } [0, T] \times \partial\Omega_i \\ u_n^i(0, x) = u_0^i(x, \lambda_i, \lambda_j), & \text{in } \Omega_i \\ \text{for all } i, j = 1, 2 \text{ and } i \neq j. & \end{array} \right. \quad (11)$$

We look for approximate solutions (u_n^i) for the problem (11) in the form

$$u_n^i(t, x) = \sum_{k=1}^n d_k^i(t) v_k, \quad \text{for } i = 1, 2. \quad (12)$$

Multiplying equation (11) with function test v_k formulates the following Galerkin variational formulation for our problem:

$$\left\{ \begin{array}{l} \int_{\Omega_i} \partial_t u_n^i v_k + \int_{\Omega_i} A_i(\lambda_i) \nabla u_n^i \nabla v_k + \int_{\Omega_i} A_j(\lambda_j) \nabla u_n^j \nabla v_k = \int_{\Omega_i} g(u_n^i, u_n^j) v_k \\ \quad + \int_{\Gamma} \alpha^j (I_n^i) u_n^j v_k + \int_{\Omega_i} \lambda_j u_n^j v_k - \int_{\Omega_i} \lambda_i u_n^i v_k, \\ \text{for all } i, j = 1, 2 \text{ and } i \neq j. \end{array} \right. \quad (13)$$

Substituting (12) into (13) leads to the ODE system: for all $i, j = 1, 2$ and $i \neq j$ we have

$$\mathbf{M}_i (d_k^i)' + \mathbf{K}_i d_k^i + \mathbf{K}_j d_k^j = \mathbf{G}(d_k^i, d_k^j) + \lambda_j \mathbf{M}_i d_k^j - \lambda_i \mathbf{M}_i d_k^i \quad (14)$$

for all $i, j = 1, 2, i \neq j$ and $k = 1, 2, \dots, n$.

where \mathbf{M}_i denotes the mass matrix, \mathbf{K}_i the stiffness matrix, and \mathbf{G} represents the nonlinear reaction component. It may be useful to explicitly define these terms as

follows:

$$\begin{aligned}
[\mathbf{M}_i]_{kl} &= \int_{\Omega_i} v_l v_k dx, \\
[\mathbf{K}_i]_{kl} &= \int_{\Omega_i} A_i(\lambda_i) \nabla v_l \cdot \nabla v_k dx, \\
[\mathbf{G}(d^i, d^j)]_k &= \int_{\Omega_i} g \left(\sum_{l=1}^n d_l^i v_l, \sum_{m=1}^n d_m^j v_m \right) v_k dx + \int_{\Gamma} \alpha^j(I_n^i) \left(\sum_{m=1}^n d_m^j v_m \right) v_k dy.
\end{aligned}$$

This coupled differential system can be completed with the initial conditions

$$d_k^i(0) = \langle u_0, v_k \rangle_{L^2(\Omega)}, \quad \text{for all } i = 1, 2 \text{ and } k = 1, \dots, n, \quad (15)$$

Thanks to the global Lipschitz condition on g and the boundedness of α^j , the standard theory of ordinary differential equations provides the local existence and uniqueness of solutions $\left(d_1^i(t), d_2^i(t), \dots, d_n^i(t) \right)$, where $i = 1, 2$ for the differential system (14)-(15). Hence, there exists a unique local solution (u_n^1, u_n^2) of (13).

Step 2: Estimation of (u_n^1, u_n^2) :

The next step is concerned with establishing energy estimates for the solution u_n and its derivatives. Starting by taking $v_k = u_n^1$ for $i = 1$ and $v_k = u_n^2$ for $i = 2$ in equation (13), we obtain:

$$\begin{aligned}
\int_{\Omega_1} \partial_t u_n^1 u_n^1 + \int_{\Omega_1} A_1(\lambda_1) \nabla u_n^1 \nabla u_n^1 + \int_{\Omega_1} A_2(\lambda_2) \nabla u_n^2 \nabla u_n^1 &= \int_{\Omega_1} g(u_n^1, u_n^2) u_n^1 + \\
&\int_{\Gamma} \alpha(I_n^1) u_n^1 u_n^1 + \int_{\Omega_1} \lambda_2 u_n^2 u_n^1 - \int_{\Omega_1} \lambda_1 u_n^1 u_n^1, \\
\int_{\Omega_2} \partial_t u_n^2 u_n^2 + \int_{\Omega_2} A_2(\lambda_2) \nabla u_n^2 \nabla u_n^2 + \int_{\Omega_2} A_1(\lambda_1) \nabla u_n^1 \nabla u_n^2 &= \int_{\Omega_2} g(u_n^2, u_n^1) u_n^2 + \\
&\int_{\Gamma} \alpha(I_n^2) u_n^2 u_n^2 + \int_{\Omega_2} \lambda_1 u_n^1 u_n^2 - \int_{\Omega_2} \lambda_2 u_n^2 u_n^2.
\end{aligned} \quad (16)$$

Summing the two equations, and using Young's inequality (given that $\lambda_i \in [0, 1]$),

yields:

$$\begin{aligned}
\int_{\Omega_1} \partial_t u_n^1 u_n^1 + \int_{\Omega_2} \partial_t u_n^2 u_n^2 + \|u_n^1\|_{\mathbf{H}^1_{A_1,0}(\Omega_1)}^2 + \|u_n^2\|_{\mathbf{H}^1_{A_2,0}(\Omega_2)}^2 &\leq \int_{\Omega_2} g(u_n^2, u_n^1) u_n^2 + \|u_n^1\|_{\mathbf{L}^2(\Omega_1)}^2 + \\
\|u_n^2\|_{\mathbf{L}^2(\Omega_2)}^2 + \int_{\Omega_1} g(u_n^1, u_n^2) u_n^1 + \frac{\epsilon}{2} \|\lambda_1 u_n^1\|_{\mathbf{L}^2(\Omega_2)}^2 + \frac{1}{2\epsilon} \|u_n^2\|_{\mathbf{L}^2(\Omega_2)}^2 + \frac{1}{2\epsilon} \|u_n^1\|_{\mathbf{L}^2(\Omega_1)}^2 & \\
+ \frac{\epsilon}{2} \|\lambda_2 u_n^2\|_{\mathbf{L}^2(\Omega_1)}^2 - \int_{\Omega_1} A_2(\lambda_2) \nabla u_n^2 \nabla u_n^1 - \int_{\Omega_2} A_1(\lambda_1) \nabla u_n^1 \nabla u_n^2 & \\
\int_{\Gamma} \alpha(I_n^1)(u_n^1)^2 + \alpha(I_n^2)(u_n^2)^2 &
\end{aligned}$$

Let us estimate the terms $\int_{\Omega_1} A_2(\lambda_2) \nabla u_n^2 \nabla u_n^1$ and $\int_{\Omega_2} A_1(\lambda_1) \nabla u_n^1 \nabla u_n^2$. By the Young inequality with $\epsilon > 0$, we have

$$(\star) \quad \left| \int_{\Omega_1} A_2(\lambda_2) \nabla u_n^2 \nabla u_n^1 \right| \leq \frac{\epsilon}{2} \int_{\Omega_1} |\sqrt{A_2(\lambda_2)} \nabla u_n^2|^2 + \frac{1}{2\epsilon} \int_{\Omega_1} |\sqrt{A_2(\lambda_2)} \nabla u_n^1|^2$$

and similarly

$$(\star\star) \quad \left| \int_{\Omega_2} A_1(\lambda_1) \nabla u_n^1 \nabla u_n^2 \right| \leq \frac{\epsilon}{2} \int_{\Omega_2} |\sqrt{A_1(\lambda_1)} \nabla u_n^1|^2 + \frac{1}{2\epsilon} \int_{\Omega_2} |\sqrt{A_1(\lambda_1)} \nabla u_n^2|^2$$

By (\star) and $(\star\star)$, we obtain:

$$\begin{aligned}
\int_{\Omega_1} \partial_t u_n^1 u_n^1 + \int_{\Omega_2} \partial_t u_n^2 u_n^2 + \left(1 - \frac{1}{2\epsilon}\right) \|u_n^1\|_{\mathbf{H}^1_{A_1,0}(\Omega_1)}^2 + \left(1 - \frac{1}{2\epsilon}\right) \|u_n^2\|_{\mathbf{H}^1_{A_2,0}(\Omega_2)}^2 &\leq \|u_n^1\|_{\mathbf{L}^2(\Omega_1)}^2 + \\
\|u_n^2\|_{\mathbf{L}^2(\Omega_2)}^2 + \|g(u_n^2, u_n^1)\|_{\mathbf{L}^2(\Omega_2)} \|u_n^2\|_{\mathbf{L}^2(\Omega_2)} + \|g(u_n^1, u_n^2)\|_{\mathbf{L}^2(\Omega_1)} \|u_n^1\|_{\mathbf{L}^2(\Omega_1)} & \\
+ \frac{\epsilon}{2} \|\lambda_1 u_n^1\|_{\mathbf{L}^2(\Omega_2)}^2 + \frac{\epsilon}{2} \|\lambda_2 u_n^2\|_{\mathbf{L}^2(\Omega_1)}^2 + C_{\Gamma} \|u_n^1\|_{\mathbf{L}^2(\Omega_1)}^2 + C_{\Gamma} \|u_n^2\|_{\mathbf{L}^2(\Omega_2)}^2 &
\end{aligned}$$

$C_{\Gamma} > 0$ is derived from the trace theorems.

Since g is a globally Lipschitz function satisfying $g(0, 0) = 0$, and by the definition and properties of the operator \mathcal{I} , we obtain:

$$\begin{aligned}
\int_{\Omega_1} \partial_t u_n^1 u_n^1 + \int_{\Omega_2} \partial_t u_n^2 u_n^2 + \left(1 - \frac{1}{2\epsilon}\right) \|u_n^1\|_{\mathbf{H}^1_{A_1,0}(\Omega_1)}^2 + \left(1 - \frac{1}{2\epsilon}\right) \|u_n^2\|_{\mathbf{H}^1_{A_2,0}(\Omega_2)}^2 &\leq \\
\left(1 + L_g + \frac{\epsilon}{2} M_{\mathcal{I}}^2 + C_{\Gamma}\right) \|(u_n^1, u_n^2)\|_{\mathbf{L}^2(\Omega_1) \times \mathbf{L}^2(\Omega_2)}^2 &
\end{aligned}$$

Then

$$\int_{\Omega_1} \partial_t u_n^1 u_n^1 + \int_{\Omega_2} \partial_t u_n^2 u_n^2 + \left(1 - \frac{1}{2\epsilon}\right) \|(u_n^1, u_n^2)\|_{\mathbf{H}_{A_1,0}^1(\Omega_1) \times \mathbf{H}_{A_2,0}^1(\Omega_2)}^2 \leq \left(1 + L_g + \frac{\epsilon}{2} M_{\mathcal{I}}^2 + C_{\Gamma}\right) \|(u_n^1, u_n^2)\|_{\mathbf{L}^2(\Omega_1) \times \mathbf{L}^2(\Omega_2)}^2.$$

Choosing $\epsilon > 0$ so that $\epsilon > \frac{1}{2}$, we have

$$\frac{1}{2} \frac{d}{dt} \|(u_n^1(\cdot, s), u_n^2(\cdot, s))\|_{\mathbf{L}^2(\Omega_1) \times \mathbf{L}^2(\Omega_2)}^2 + \|(u_n^1, u_n^2)\|_{\mathbf{H}_{A_1,0}^1(\Omega_1) \times \mathbf{H}_{A_2,0}^1(\Omega_2)}^2 \leq M_2 \|(u_n^1, u_n^2)\|_{\mathbf{L}^2(\Omega_1) \times \mathbf{L}^2(\Omega_2)}^2 \quad (17)$$

and thus

$$\frac{1}{2} \frac{d}{dt} \|(u_n^1(\cdot, s), u_n^2(\cdot, s))\|_{\mathbf{L}^2(\Omega_1) \times \mathbf{L}^2(\Omega_2)}^2 \leq M_2 \|(u_n^1, u_n^2)\|_{\mathbf{L}^2(\Omega_1) \times \mathbf{L}^2(\Omega_2)}^2.$$

Gronwall's lemma yields the existence of a constant $\tilde{C} > 0$ such that:

$$\|(u_n^1(\cdot, t), u_n^2(\cdot, t))\|_{\mathbf{L}^2(\Omega_1) \times \mathbf{L}^2(\Omega_2)}^2 \leq \tilde{C} := e^{2M_2 t} \|(u_n^1(\cdot, 0), u_n^2(\cdot, 0))\|_{\mathbf{L}^2(\Omega_1) \times \mathbf{L}^2(\Omega_2)}^2 \quad (18)$$

we can get the following estimation

$$\max_{0 \leq t \leq T} \|(u_n^1(\cdot, t), u_n^2(\cdot, t))\|_{\mathbf{L}^2(\Omega_1) \times \mathbf{L}^2(\Omega_2)}^2 \leq \tilde{C} := e^{2M_2 T} \|(u_n^1(\cdot, 0), u_n^2(\cdot, 0))\|_{\mathbf{L}^2(\Omega_1) \times \mathbf{L}^2(\Omega_2)}^2 \quad (19)$$

Returning once more to inequality (17), we integrate 0 and T and the employ the inequality above to find

$$\begin{aligned} \|(u_n^1, u_n^2)\|_{\mathbf{L}^2(0,T, \mathbf{H}_{A_1,0}^1(\Omega_1)) \times \mathbf{L}^2(0,T, \mathbf{H}_{A_2,0}^1(\Omega_2))}^2 &= \int_0^T \|u_n^1, u_n^2\|_{\mathbf{H}_{A_1,0}^1(\Omega_1) \times \mathbf{H}_{A_2,0}^1(\Omega_2)}^2 dt \\ &\leq \tilde{C}_1 := \frac{e^{2M_2 T} - 1}{2M_2} \|(u_n^1(\cdot, 0), u_n^2(\cdot, 0))\|_{\mathbf{L}^2(\Omega_1) \times \mathbf{L}^2(\Omega_2)}^2 \end{aligned} \quad (20)$$

The inequality (20) implies that $(u_n^1, u_n^2)_n$ is a bounded sequence in $\mathbf{L}^2(0, T, \mathbf{H}_{A_1,0}^1(\Omega_1)) \times \mathbf{L}^2(0, T, \mathbf{H}_{A_2,0}^1(\Omega_2))$ and bounded in $L^\infty(0, T, \mathbf{L}^2(\Omega_1)) \times L^\infty(0, T, \mathbf{L}^2(\Omega_2))$ using the operator \mathcal{I} .

Step 3: Estimation of $(\partial_t u_n^1, \partial_t u_n^2)$:

Fix any $v_i \in \mathbf{H}_{A_i,0}^1(\Omega_i)$, with $\|v_i\|_{\mathbf{H}_{A_i,0}^1(\Omega_i)} \leq 1$ and $i = 1, 2$, such that $v_i = v_i^1 + v_i^2$, where $v_i^1 \in \text{span}\{v_{i,k}\}_{k=1}^n$ and $(v_i^2, v_{i,k}) = 0$ ($k = 1, \dots, n$). Since the functions

$\{v_{i,k}\}_{k=0}^{\infty}$ are orthogonal in $\mathbf{H}_{A_i,0}^1(\Omega_i)$, we have $\|v_i^1\|_{\mathbf{H}_{A_i,0}^1(\Omega_i)} \leq \|v_i\|_{\mathbf{H}_{A_i,0}^1(\Omega_i)} \leq 1$. Utilizing (13), we deduce :

$$\begin{aligned} \int_{\Omega_1} \partial_t u_n^1 v_1^1 &= - \int_{\Omega_1} A_1(\lambda_1) \nabla u_n^1 \nabla v_1^1 - \int_{\Omega_1} A_2(\lambda_2) \nabla u_n^2 \nabla v_1^1 + \int_{\Omega_1} g(u_n^1, u_n^2) v_1^1 + \\ &\quad \int_{\Gamma} \alpha(I_n^1) u_n^1 v_1^1 + \int_{\Omega_1} \lambda_2 u_n^2 v_1^1 - \int_{\Omega_1} \lambda_1 u_n^1 v_1^1, \\ \int_{\Omega_2} \partial_t u_n^2 v_2^1 &= - \int_{\Omega_2} A_2(\lambda_2) \nabla u_n^2 \nabla v_2^1 - \int_{\Omega_2} A_1(\lambda_1) \nabla v_2^1 \nabla v_1^1 + \int_{\Omega_2} g(u_n^2, u_n^1) v_2^1 + \\ &\quad \int_{\Gamma} \alpha(I_n^2) u_n^2 v_2^1 + \int_{\Omega_2} \lambda_1 u_n^1 v_2^1 - \int_{\Omega_2} \lambda_2 u_n^2 v_2^1, \end{aligned} \quad (21)$$

Then the definition (12) of u_n implies

$$\begin{aligned} \langle \partial_t u_n^1, v_1 \rangle &= \langle \partial_t u_n^1, v_1^1 \rangle = - \int_{\Omega_1} A_1(\lambda_1) \nabla u_n^1 \nabla v_1^1 - \int_{\Omega_1} A_2(\lambda_2) \nabla u_n^2 \nabla v_1^1 + \int_{\Omega_1} g(u_n^1, u_n^2) v_1^1 + \\ &\quad \int_{\Gamma} \alpha(I_n^1) u_n^1 v_1^1 + \int_{\Omega_1} \lambda_2 u_n^2 v_1^1 - \int_{\Omega_1} \lambda_1 u_n^1 v_1^1, \\ \langle \partial_t u_n^2, v_2 \rangle &= \langle \partial_t u_n^2, v_2^1 \rangle = - \int_{\Omega_2} A_2(\lambda_2) \nabla u_n^2 \nabla v_2^1 - \int_{\Omega_2} A_1(\lambda_1) \nabla v_2^1 \nabla v_1^1 + \int_{\Omega_2} g(u_n^2, u_n^1) v_2^1 + \\ &\quad \int_{\Gamma} \alpha(I_n^2) u_n^2 v_2^1 + \int_{\Omega_2} \lambda_1 u_n^1 v_2^1 - \int_{\Omega_2} \lambda_2 u_n^2 v_2^1, \end{aligned} \quad (22)$$

Consequently

$$\begin{aligned} |\langle \partial_t u_n^1, v_1 \rangle| &\leq C^1(u_n^{1,2}) \|v_1^1\|_{\mathbf{H}_{A_1,0}^1(\Omega_1)} \\ |\langle \partial_t u_n^2, v_2 \rangle| &\leq C^2(u_n^{1,2}) \|v_2^1\|_{\mathbf{H}_{A_2,0}^1(\Omega_2)} \end{aligned}$$

where

$$C^1(u_n^{1,2}) = \left(\|u_n^1\|_{\mathbf{H}_{A_1,0}^1(\Omega_1)} + \|u_n^2\|_{\mathbf{H}_{A_1,0}^1(\Omega_1)} + L_g \|u_n^1\|_{\mathbf{L}^2(\Omega_1)} + \|u_n^2\|_{\mathbf{L}^2(\Omega_1)} + \|u_n^1\|_{\mathbf{L}^2(\Omega_1)} \right)$$

and

$$C^2(u_n^{1,2}) = \left(\|u_n^2\|_{\mathbf{H}_{A_2,0}^1(\Omega_2)} + \|u_n^1\|_{\mathbf{H}_{A_2,0}^1(\Omega_2)} + L_g \|u_n^2\|_{\mathbf{L}^2(\Omega_2)} + \|u_n^1\|_{\mathbf{L}^2(\Omega_2)} + \|u_n^2\|_{\mathbf{L}^2(\Omega_2)} \right),$$

using the operator \mathcal{I} and since $\|v_i^1\|_{\mathbf{H}_{A_i,0}^1(\Omega_i)} \leq 1$. Thus

$$\|(\partial_t u_n^1, \partial_t u_n^2)\|_{\mathbf{H}_{A_1,0}^{-1}(\Omega_1) \times \mathbf{H}_{A_2,0}^{-1}(\Omega_2)} \leq \hat{C}_2 \|(u_n^1, u_n^2)\|_{\mathbf{H}_{A_1,0}^1(\Omega_1) \times \mathbf{H}_{A_2,0}^1(\Omega_2)},$$

and therefore

$$\begin{aligned} \|(\partial_t u_n^1, \partial_t u_n^2)\|_{\mathbf{L}^2(0,T, \mathbf{H}_{A_1,0}^{-1}(\Omega_1)) \times \mathbf{L}^2(0,T, \mathbf{H}_{A_2,0}^{-1}(\Omega_2))} &= \int_0^T (\partial_t u_n^1, \partial_t u_n^2)_{\mathbf{H}_{A_1,0}^{-1}(\Omega_1) \times \mathbf{H}_{A_2,0}^{-1}(\Omega_2)}^2 dt \\ &\leq \hat{C}_2 \int_0^T \|(u_n^1, u_n^2)\|_{\mathbf{H}_{A_1,0}^1(\Omega_1) \times \mathbf{H}_{A_2,0}^1(\Omega_2)}^2 dt \leq \hat{C}_2 \hat{C}_1 \end{aligned} \quad (23)$$

the inequality (23) implies that $(\partial_t u_n^1, \partial_t u_n^2)_n$ is bounded in $\mathbf{L}^2(0, T, \mathbf{H}_{A_1,0}^{-1}(\Omega_1)) \times \mathbf{L}^2(0, T, \mathbf{H}_{A_2,0}^{-1}(\Omega_2))$.

Step 4: Convergence

There exists a subsequence, still denoted (u_n^1, u_n^2) , such that

$$u_n^i \rightharpoonup u^i \text{ weakly in } \mathbf{L}^2(0, T, \mathbf{H}_{A_i,0}^1(\Omega)), \quad (24)$$

$$\partial_t u_n^i \rightharpoonup \partial_t u^i \text{ weakly in } \mathbf{L}^2(0, T, \mathbf{H}_{A_i,0}^{-1}(\Omega)), \quad (25)$$

Step 5: Passage to the limit

For all $i, j = 1, 2$ and $i \neq j$ we have

$$\begin{aligned} \int_0^T \langle \partial_t u_n^i, v^i \rangle_{\Omega_i} + \int_0^T \langle A_i(\lambda_i) \nabla u_n^i, \nabla v^i \rangle_{\Omega_i} + \int_0^T \langle A_j(\lambda_j) \nabla u_n^j, \nabla v^i \rangle_{\Omega_i} &= \int_0^T \langle g(u_n^i, u_n^j), v^i \rangle_{\Omega_i} + \\ &\int_0^T \langle \alpha(I_n^i) u_n^i, v^i \rangle_{\Gamma} + \int_0^T \langle \lambda_j u_n^j, v^i \rangle_{\Omega_i} - \int_0^T \langle \lambda_i u_n^i, v^i \rangle_{\Omega_i}. \end{aligned}$$

Since g is globally Lipschitz continuous and $(u_n^i)_n$ is bounded as above, By the Aubin-Lions lemma [30],

$$g(u_n^i, u_n^j) \rightarrow g(u^i, u^j) \text{ strongly in } \mathbf{L}^2(0, T, \mathbf{L}^2(\Omega_i)).$$

Similarly, this approach yields the following convergence result :

$$\alpha(I_n^i) \rightarrow \alpha(I^i) \text{ strongly in } \mathbf{L}^2(0, T, \mathbf{L}^2(\Gamma)), \quad \text{for } i = 1, 2.$$

and passing to the limit when $n \rightarrow +\infty$ in the weak formulation, for all $i, j = 1, 2$ and $i \neq j$, we obtain

$$\begin{aligned} \int_0^T \langle \partial_t u^i, v^i \rangle_{\Omega_i} + \int_0^T \langle A_i(\lambda_i) \nabla u^i, \nabla v^i \rangle_{\Omega_i} + \int_0^T \langle A_j(\lambda_j) \nabla u^j, \nabla v^i \rangle_{\Omega_i} &= \int_0^T \langle g(u^i, u^j), v^i \rangle_{\Omega_i} + \\ &\langle \int_0^T \alpha(I^i) u^i, v^i \rangle_{\Gamma} + \int_0^T \langle \lambda_j u^j, v^i \rangle_{\Omega_i} - \int_0^T \langle \lambda_i u^i, v^i \rangle_{\Omega_i}. \end{aligned}$$

for all $v \in \mathbf{L}^2(0, T, \mathbf{H}_{A_1, 0}^1(\Omega)) \times \mathbf{L}^2(0, T, \mathbf{H}_{A_2, 0}^1(\Omega))$.

Step 6: Uniqueness

Let us suppose that the problem (8) has two solutions (u^1, u^2) and (w^1, w^2) . Subtracting the weak formulations (13) of the solutions yields

$$\begin{aligned} & \int_{\Omega_1} (\partial_t u^1 - \partial_t w^1) v_1 + \int_{\Omega_1} A_1(\lambda_1) (\nabla u^1 - \nabla w^1) \nabla v_1 + \int_{\Omega_1} A_2(\lambda_2) (\nabla u^2 - \nabla w^2) \nabla v_1 + \\ & \int_{\Omega_2} (\partial_t u^2 - \partial_t w^2) v_2 + \int_{\Omega_2} A_1(\lambda_1) (\nabla u^1 - \nabla w^1) \nabla v_2 + \int_{\Omega_2} A_2(\lambda_2) (\nabla u^2 - \nabla w^2) \nabla v_2 \\ = & \int_{\Omega_1} \lambda_1 (u^2 - w^2) v_1 - \int_{\Omega_1} \lambda_1 (u^1 - w^1) v_1 + \int_{\Omega_2} \lambda_2 (u^1 - w^1) v_2 - \int_{\Omega_2} \lambda_2 (u^2 - w^2) v_2, \\ & + \int_{\Omega_1} v_1 (g(u^1, u^2) - g(w^1, w^2)) + \int_{\Omega_2} v_2 (g(u^2, u^1) - g(w^2, w^1)) + \sum_{i=1}^2 \int_{\Gamma} \alpha(I_u^i) u^i - \alpha(I_w^i) w^i, v^i \rangle_{\Gamma} \end{aligned}$$

by taking $v_i = u^i - w^i, i = 1, 2$ as a test function gives

$$\begin{aligned} & \int_{\Omega_1} \partial_t v_1 v_1 + \int_{\Omega_1} A_1(\lambda_1) \nabla v_1 \nabla v_1 + \int_{\Omega_1} A_2(\lambda_2) \nabla v_1 \nabla v_2 + \int_{\Omega_1} \partial_t v_2 v_2 + \int_{\Omega_2} A_2(\lambda_2) \nabla v_2 \nabla v_2 \\ & + \int_{\Omega_2} A_1(\lambda_1) \nabla v_1 \nabla v_2 = \int_{\Omega_1} \lambda_1 v_2 v_1 - \int_{\Omega_1} \lambda_1 v_1 v_1 + \int_{\Omega_2} \lambda_2 v_1 v_2 - \int_{\Omega_2} \lambda_2 v_2 v_2, \\ & + \int_{\Omega_1} v_1 (g(u^1, u^2) - g(w^1, w^2)) + \int_{\Omega_2} v_2 (g(u^2, u^1) - g(w^2, w^1)) + \sum_{i=1}^2 \int_{\Gamma} \alpha(I_u^i) u^i - \alpha(I_w^i) w^i, v^i \rangle_{\Gamma} \end{aligned}$$

using the same technique the estimation of the approach solution sequence u_n we obtain the following estimation similar to the estimation (17)

$$\frac{1}{2} \frac{d}{dt} \|(v_1(\cdot, s), v_2(\cdot, s))\|_{\mathbf{L}^2(\Omega_1) \times \mathbf{L}^2(\Omega_2)}^2 + \|(v_1, v_2)\|_{\mathbf{H}_{A_1, 0}^1(\Omega_1) \times \mathbf{H}_{A_2, 0}^1(\Omega_2)}^2 \leq M_v \|(v_1, v_2)\|_{\mathbf{L}^2(\Omega_1) \times \mathbf{L}^2(\Omega_2)}^2 \quad (26)$$

Applying the Gronwall's lemma gives

$$v_i = 0 \text{ a. e. in } Q_i.$$

□

before proving the theorem (1), we know that the reaction function $f : \mathbf{H}_{A_1}^1(\Omega) \times \mathbf{H}_{A_2}^1(\Omega) \rightarrow \mathbf{L}^2(\Omega) \times \mathbf{L}^2(\Omega)$ is locally Lipschitz, we use a standard truncation of the source as follows, for all $u = (u^1, u^2)$:

$$\mathcal{T}r(u) = \begin{cases} f(u), & \text{if } \|u\|_{\mathbf{H}_{A_1}^1(\Omega) \times \mathbf{H}_{A_2}^1(\Omega)} \leq \delta \\ f\left(\frac{\delta u}{\|u\|_{\mathbf{H}_{A_1}^1(\Omega) \times \mathbf{H}_{A_2}^1(\Omega)}}\right), & \text{if } \|u\|_{\mathbf{H}_{A_1}^1(\Omega) \times \mathbf{H}_{A_2}^1(\Omega)} > \delta \end{cases}$$

where δ is a positive constant. it is easy to see that $\mathcal{T}r$ is globally Lipschitz with a Lipschitz constant $L_{\mathcal{T}r} > 0$ and it satisfies $\mathcal{T}r(0, 0) = 0$.

Proof of the theorem (1). The function $\mathcal{T}r$ verifies the same hypotheses of the function g define in the proposition (2), which means that the following truncated problem has a unique solution $u_\delta = (u_\delta^1, u_\delta^2)$

$$\left\{ \begin{array}{ll} \partial_t u_\delta^i - \operatorname{div}(A_i(\lambda_i) \nabla u_\delta^i) = \mathcal{T}r(u_\delta^i, u_\delta^j) + \operatorname{div}(A_j(\lambda_j) \nabla u_\delta^j) + \lambda_j u_\delta^j - \lambda_i u_\delta^i, & \text{in } [0, T] \times \Omega_i \\ A_i(\lambda_i) \nabla u_\delta^i \cdot \tau + A_j(\lambda_j) \nabla u_\delta^j \cdot \tau + \alpha^j (I^i) u_\delta^j = \mathbf{0}, & \text{on } [0, T] \times \Gamma \\ u_\delta^i = \mathbf{0} & \text{on } [0, T] \times \partial\Omega_i \\ u_\delta^i(0, x) = u_0^i(x, \lambda_i, \lambda_j) & \text{in } \Omega_i \\ \text{for all } i, j = 1, 2 \text{ and } i \neq j. & \end{array} \right. \quad (27)$$

According to the Proposition (2), (u_δ^1, u_δ^2) satisfies the following energy inequality:

$$\|(u_\delta^1, u_\delta^2)\|_{\mathbf{L}^2(0, T, \mathbf{H}_{\lambda_1, 0}^1(\Omega_1)) \times \mathbf{L}^2(0, T, \mathbf{H}_{\lambda_2, 0}^1(\Omega_2))}^2 \leq \bar{C}_\delta \|u_\delta^1(\cdot, 0), u_\delta^2(\cdot, 0)\|_{\mathbf{L}^2(\Omega_1) \times \mathbf{L}^2(\Omega_2)}^2 \quad (28)$$

Choosing $\bar{C}_\delta \|u_\delta^1(\cdot, 0), u_\delta^2(\cdot, 0)\|_{\mathbf{L}^2(\Omega_1) \times \mathbf{L}^2(\Omega_2)}^2 \leq \delta$ leads to prove $\mathcal{T}r(u) = f(u)$ given in the initial problem.

Let's now prove the positivity of the solution of our problem, by rewriting u_δ^i as follow $u_\delta^i = (\xi^i)^+ - (\xi^i)^-$ where $(\xi^i)^+, (\xi^i)^- \geq 0$, they are defined by

$$(\xi^i)^+ := \max(0, u_\delta^i) \text{ and } (\xi^i)^- := \max(0, -u_\delta^i)$$

By using the estimation of solution proven in (28), we get

$$\|(\xi^1)^-(\cdot, t)\|_{L^2(\Omega_1)}^2 + \|(\xi^2)^-(\cdot, t)\|_{L^2(\Omega_2)}^2 \leq \left(\|(\xi^1)^-(\cdot, 0)\|_{L^2(\Omega_1)}^2 + \|(\xi^2)^-(\cdot, 0)\|_{L^2(\Omega_2)}^2 \right) \bar{C}_\delta.$$

Since $u_0^i > 0$ which means that $(\xi^i)^-(\cdot, 0) := (\xi_0^i)^- = 0$, last estimation yields to $(\xi^i)^-(\cdot, t) = 0$ then the positivity of solution is proven. \square

4 Finite Volume Method (FVM)

To approximate the solution of problem (6) by means of the Finite Volume Method (FVM), we discretize both the spatial domain and the temporal interval. The computational domain Ω is partitioned into N_x control volumes (cells) of uniform size

Δx . The center of the i -th control volume is denoted by x_i , while its left and right interfaces are represented by $x_{i-\frac{1}{2}}$ and $x_{i+\frac{1}{2}}$, respectively.

We integrate our problem (6) over a control volume $[x_{i-\frac{1}{2}}, x_{i+\frac{1}{2}}]$ to obtain the following finite volume formulation:

$$\begin{aligned} \int_{x_{i-\frac{1}{2}}}^{x_{i+\frac{1}{2}}} \partial_t u^i dx &= \int_{x_{i-\frac{1}{2}}}^{x_{i+\frac{1}{2}}} \operatorname{div}(A_i(\lambda_i) \nabla u^i) dx + \int_{x_{i-\frac{1}{2}}}^{x_{i+\frac{1}{2}}} f(u^i, u^j) dx \\ &+ \int_{x_{i-\frac{1}{2}}}^{x_{i+\frac{1}{2}}} \operatorname{div}(A_j(\lambda_j) \nabla u^j) dx + \int_{x_{i-\frac{1}{2}}}^{x_{i+\frac{1}{2}}} \lambda_j u^j dx - \int_{x_{i-\frac{1}{2}}}^{x_{i+\frac{1}{2}}} \lambda_i u^i dx \end{aligned} \quad (29)$$

The right-hand side can be simplified using the divergence theorem:

$$\int_{x_{i-\frac{1}{2}}}^{x_{i+\frac{1}{2}}} \operatorname{div}(A_i(\lambda_i) \nabla u^i) dx = [A_i(\lambda_i) \nabla u^i \cdot \tau]_{x_{i-\frac{1}{2}}}^{x_{i+\frac{1}{2}}}$$

Let us define the discrete solution u^i with the following approximated formula:

$$U_j^{i,n} \approx u^i(x_j, t_n), \quad \text{for } j = 1, \dots, N_x. \quad (30)$$

In the Finite Volume Method, the fluxes $\Psi_{i+\frac{1}{2}}$ represent the transfer of the conserved quantity across the interfaces of the control volumes. These fluxes play a central role in ensuring local conservation and are typically approximated using suitable numerical schemes. In the case of a degenerate diffusion coefficient $A_i(\lambda_i)$, the flux at the boundaries of each control volume can be approximated as:

$$\Psi_{i+\frac{1}{2}} = A_i(\lambda_i) \frac{u_{i+1} - u_i}{\Delta x}$$

This approximation is based on the first-order finite difference approximation of the gradient of u across the cell interface.

The fluxes $\Psi_{i+\frac{1}{2}}$ are used to rewrite the problem (29) as the discrete system of equations in matrix form:

$$\frac{dU^{i,n+1}}{dt} + K_i U^{i,n+1} = F_i(U^{i,n+1}, U^{j,n+1}), \quad (31)$$

where:

- K is the matrix, assembled from numerical flux approximations:

$$K_{i,i-1} = -\frac{A_i(\lambda_i)}{(\Delta x)^2}, \quad K_{i,i} = \frac{A_i(\lambda_i) + A_i(\lambda_i)}{(\Delta x)^2}, \quad K_{i,i+1} = -\frac{A_i(\lambda_i)}{(\Delta x)^2}.$$

- $F_i(U^{i,n+1}, U^{j,n+1})$ contains nonlinear terms and coupling effects.

To advance the solution in time, we use the implicit Euler method:

$$\frac{U^{i,n+1} - U^{i,n}}{\Delta t} + K_i U^{i,n+1} = F_i(U^{i,n+1}, U^{j,n+1}), \quad (32)$$

where Δt is the time step size.

The coupled system is solved iteratively using the following steps:

1. **Solve for $U^{1,n+1}$:**

$$\frac{U^{1,n+1} - U^{1,n}}{\Delta t} + K_1 U^{1,n+1} = F_1(U^{1,n}, U^{2,n}). \quad (33)$$

2. **Use the solution of $U^{1,n+1}$ to solve for $U^{2,n+1}$:**

$$\frac{U^{2,n+1} - U^{2,n}}{\Delta t} + K_2 U^{2,n+1} = F_2(U^{2,n}, U^{1,n+1}). \quad (34)$$

These steps ensure that the solution at each time step remains consistent with the governing equations and coupling conditions.

5 Numerical Results

This section presents the numerical results of the model in a one-dimensional (1D) spatial domain. The domain is divided into two subdomains: $\Omega_1 =]0, 1]$ and $\Omega_2 = [1, 2[$. Each subdomain is discretized using $N_x = 302$ spatial points. The simulations are conducted over a time interval of $T = 300$ days, with a time step size of $\Delta t = 0.0125$ days. They are performed using the specified initial conditions and parameter values detailed below.

The initial population in each subdomain is set as follows:

- **In the subdomain $\Omega_1 =]0, 1]$:** The susceptible population (S_1) is uniformly distributed with an initial normalized value of 0.8 (240 individuals), the infected population (I_1) is uniformly distributed with an initial normalized value of 0.2 (60 individuals), and the recovered population (R_1) is initially zero.
- **In the subdomain $\Omega_2 = [1, 2[$:** The susceptible population (S_2) is uniformly distributed with an initial normalized value of 1.0 (300 individuals), while both the infected population (I_2) and the recovered population (R_2) are initially zero.

The parameter λ_j denotes the probability that an individual originating from subdomain Ω_j resides in subdomain Ω_i , thereby accounting for immigration before disease detection. To model this probability, we employ, for instance, a spatial Poisson process, as described in [26]. This choice is motivated by the need to capture both the spatial variability of population's movements and the inherent randomness of individual migration patterns. A spatial Poisson process provides a flexible framework for representing the distribution of individuals across the domain, thereby allowing the incorporation of spatial heterogeneity into the infection dynamics. Through this approach, we can simulate how the probability of an individual being located in a given subdomain varies spatially, thus reflecting more realistic scenarios where population movement is inherently non-uniform.

For our simulations, we consider a simple yet illustrative example where we define the probability function $\lambda_i(x)$ as:

$$\lambda_1(x) = \begin{cases} 0, & \text{if } x = 0, \\ \lambda, & \text{otherwise.} \end{cases} \quad \text{and} \quad \lambda_2(x) = \begin{cases} 0, & \text{if } x = 2 \\ \lambda, & \text{otherwise.} \end{cases}$$

This configuration enables us to investigate the impact of uniform immigration probabilities in the interior regions while taking into account potential barriers or restrictions at the domain edges.

The key parameters used in the simulations are summarized in Table 1. These parameters are critical in determining the dynamics of the model and are chosen based on realistic epidemiological scenarios.

Table 1: Model Parameters

Parameter	β_1	β_2	β_{ij}	γ_1	γ_2	Λ_1	Λ_2	μ_S	μ_I	μ_R	λ
Value (day ⁻¹)	0.05	0.05	0.1	0.2	0.2	0.005	0.005	0.05	0.13	0.05	0.01

The diffusion coefficient function $\sigma(y, t, \lambda)$ is a critical component in modelling the spread of the disease. It describes how the disease spreads through the spatial domain over time. The choice of $\sigma(y, t, \lambda)$ can significantly influence the model's behavior. Here, we present the chosen form of the diffusion coefficient function

$$\sigma(y, t, \lambda) = \lambda(2 - y)y \cdot e^{-a \cdot (t - t_a)} \tag{35}$$

where a and t_a are given parameters

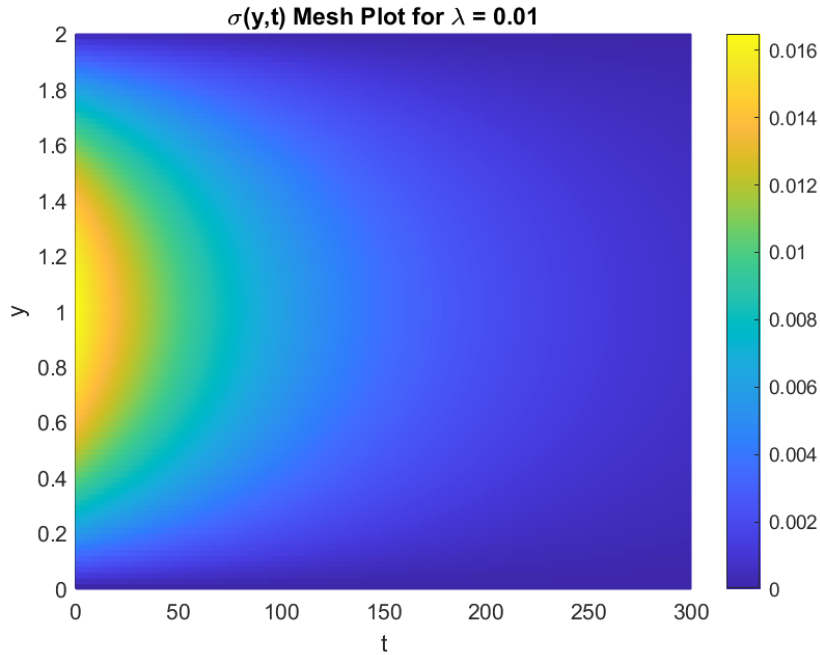
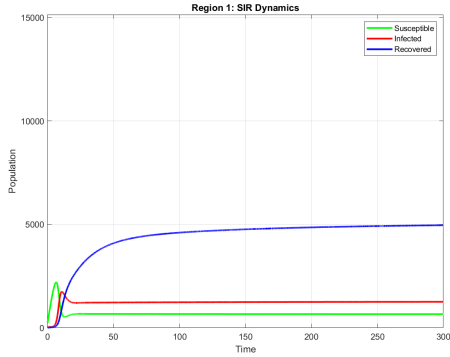


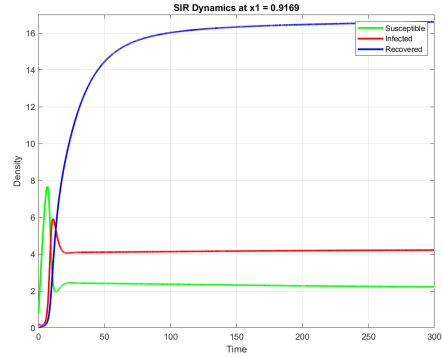
Figure 2: Diffusion coefficient function $\sigma(y, t)$ for $\lambda = 0.01$, $a = 0.01$ and $t_a = 50$.

This form ensures that the diffusion coefficient decreases exponentially over time, as shown in the figure 2 starting from a peak at $t = t_a$ days. The term $e^{-a \cdot (t-t_a)}$ captures this temporal decay. The spatial variation is governed by the term $(2-y)y$, which is a quadratic function of y . This quadratic term ensures that the diffusion coefficient is highest at $y = 1$ and decreases as y approaches 0 or 2. This choice is particularly useful for modelling scenarios where the diffusion rate decreases over time and has a peak at a specific point in the spatial domain, symmetrically decreasing as you move away from that point.

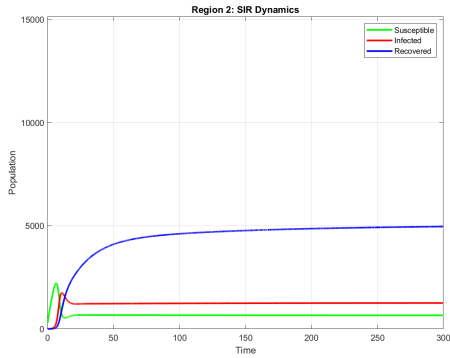
The figures illustrate the SIR dynamics for regions Ω_1 and Region Ω_2 over time, showing both the general temporal trends and the evolution at fixed spatial positions within each domain. This dual approach highlights how the combined susceptible, infected, and recovered populations change over time at specific locations. The results are further supported by heatmaps (Figures (4a),(4b) and (4c)), which provide a comprehensive spatial and temporal visualization of the solution for each compartment, clearly showing the distribution and evolution of susceptible, infected, and recovered populations across the entire domain. Figure (4d) shows the total population's evolution over time for both regions, highlighting an initial increase due to births and immigration, followed by stabilization as these factors balance with migration and deaths, reaching equilibrium.



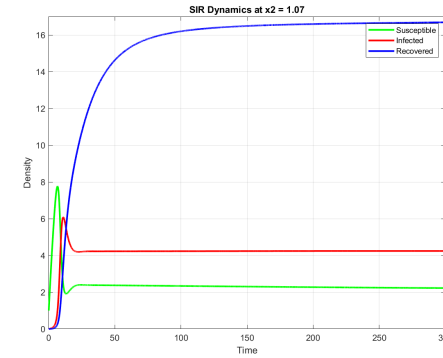
(a) SIR in Ω_1



(b) SIR evolution in a fixed point in Ω_1



(c) SIR in Ω_2



(d) SIR evolution in a fixed point in Ω_2

Figure 3: SIR model in Ω_1 and Ω_2

The table 2 demonstrates how varying the parameter λ influences key epidemic metrics across different regions. As λ increases, the peak number of infected individuals decreases significantly, from 3673 at $\lambda = 10^{-5}$ to 2012 at $\lambda = 1$. Similarly, both the total recovered individuals and total population size decrease with higher λ values, indicating a more dispersed disease impact. Importantly, lockdown requirements increase dramatically with higher λ , with lockdown duration extending from approximately 15 days at $\lambda = 10^{-5}$ to nearly 260 days at $\lambda = 1$. These findings highlight the complex relationship between population movement and disease control in multi-region epidemic models.

Complementing these observations, the contour plots in Figure 5 depict the trade-off between epidemic severity and lockdown duration. Moderate values of the mobility parameter strike a desirable balance—substantially reducing the infection peak while maintaining relatively short lockdown periods. In contrast, low mobility results in sharper epidemic peaks but shorter lockdowns, whereas high mobility flattens the curve at the cost of extended restrictions. These results emphasise the criti-

cal role of optimizing inter-regional movement to manage both public health and socio-economic impacts effectively.

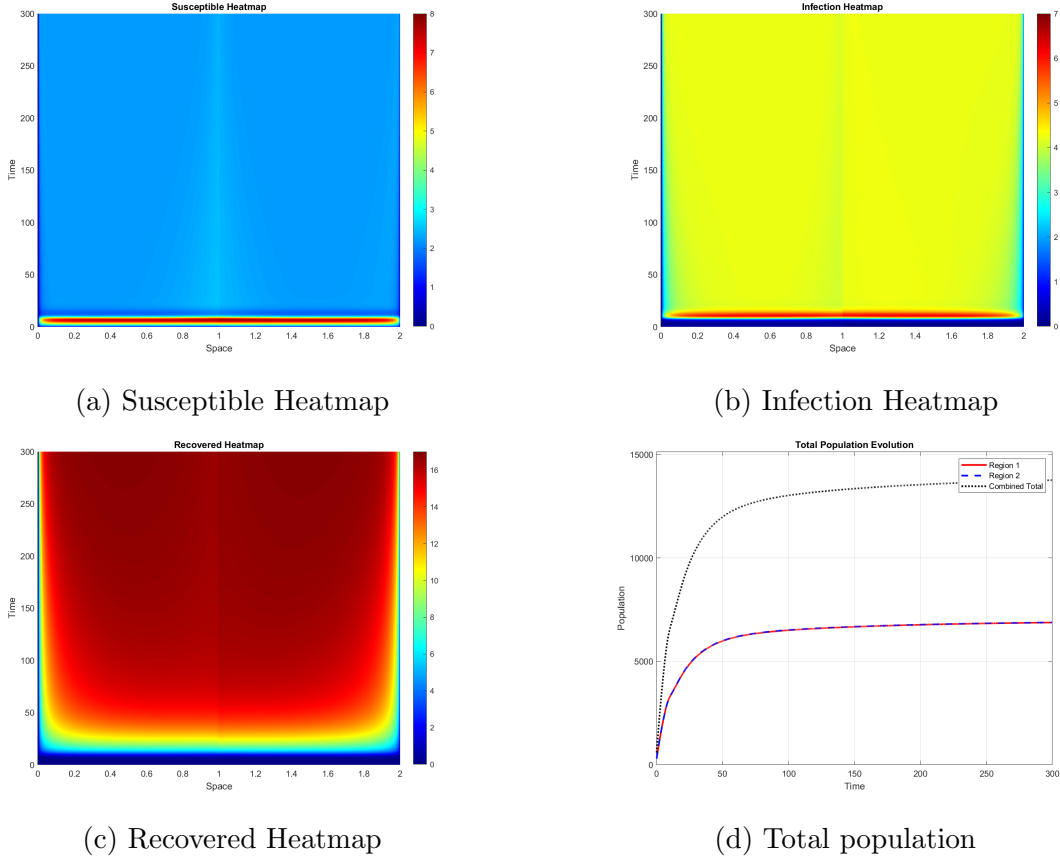
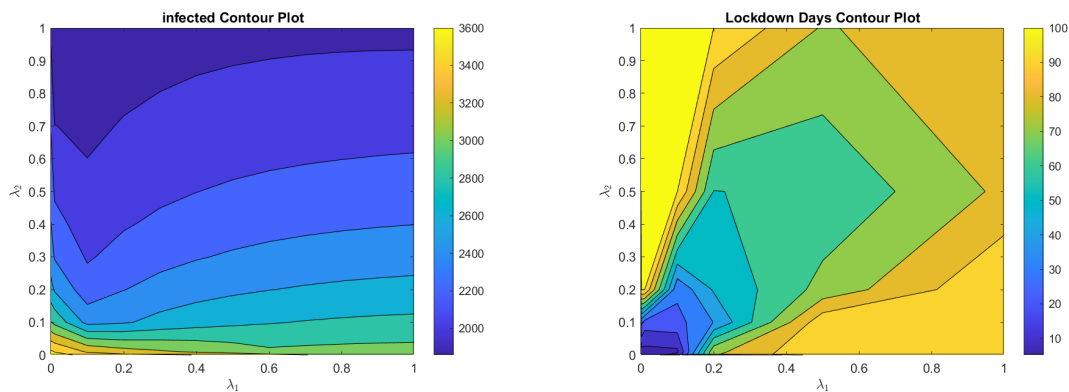


Figure 4: Heatmaps showing the spatial and temporal evolution of the SIR model, with a figure of the evolution of the total population in each subdomain

Table 2: Impact of Different λ values on proposed epidemic model

$\lambda = \lambda_1 = \lambda_2$	10^{-5}	10^{-4}	10^{-3}	10^{-2}	0.1	0.2	0.5	1
Total population	13979	13975	13947	13788	12684	11709	9623	7548
Total recovered	10125	10121	10095	9942	8880	7944	5962	4037
Peak infected	3673	3669	3645	3512	2577	2406	2251	2012
Rest infected (%)	18.10	18.11	18.13	18.27	19.40	20.55	23.39	26.65
Lockdown (days)	15.61	15.62	15.74	17.34	69.27	142.11	183.8	259.71
Lockdown (%)	5.20	5.21	5.24	5.78	23.09	47.37	61.26	86.57



(a) impact of $\lambda_{1,2}$ on the peak infected (b) impact of $\lambda_{1,2}$ on Lockdown policy

Figure 5: impact of varying λ_i , for $i = 1, 2$

Conclusion

The numerical simulations presented in this study highlight the rich spatio-temporal dynamics of the proposed degenerate SIR model. By simulating a one-dimensional domain divided into two interacting regions, we demonstrated how population movement, infection thresholds, and policy-driven boundary dynamics jointly influence the epidemic trajectory. The inclusion of degenerate diffusion captures natural mobility constraints, while the transition from Robin to Neumann boundary conditions models the enforcement of lockdowns in a mathematically consistent manner. Simulation results show the temporal evolution of each compartment, confirm theoretical predictions, and reveal the conditions under which regional isolation may mitigate disease spread. These findings underscore the model’s practical value in designing targeted interventions in spatially structured populations.

Declaration

Funding

The authors received no specific funding for this research.

Conflict of Interest

The authors declare that they have no conflict of interest.

Ethical Approval

This research did not involve human participants or animals.

Data Availability

No data were generated or analyzed during this study.

References

- [1] William Ogilvy Kermack and Anderson G McKendrick. A contribution to the mathematical theory of epidemics. *Proceedings of the royal society of london. Series A, Containing papers of a mathematical and physical character*, 115(772):700–721, 1927.
- [2] Fred Brauer, Carlos Castillo-Chavez, and Carlos Castillo-Chavez. *Mathematical models in population biology and epidemiology*, volume 2. Springer, 2012.
- [3] James Dickson Murray. *Mathematical Biology I. An Introduction*. Springer, 2002.
- [4] Pushpendra Kumar, Vedat Suat Erturk, Abdullahi Yusuf, and Sunil Kumar. Fractional time-delay mathematical modeling of oncolytic virotherapy. *Chaos, Solitons & Fractals*, 150:111123, 2021.
- [5] NH Sweilam, SM Al-Mekhlafi, ZN Mohammed, and D Baleanu. Optimal control for variable order fractional hiv/aids and malaria mathematical models with multi-time delay. *Alexandria Engineering Journal*, 59(5):3149–3162, 2020.
- [6] Priscilla E Greenwood and Luis F Gordillo. Stochastic epidemic modeling. In *Mathematical and statistical estimation approaches in epidemiology*, pages 31–52. Springer, 2009.
- [7] JAJ Metz. The epidemic in a closed population with all susceptibles equally vulnerable; some results for large susceptible populations and small initial infections. *Acta biotheoretica*, 27(1):75–123, 1978.
- [8] Carlos Castillo-Chavez, Samuel Fridman, Xiaolong Luo, et al. Stochastic and deterministic models in epidemiology. 1993.
- [9] Meksianis Z Ndi and Asep K Supriatna. Stochastic mathematical models in epidemiology. *Information*, 20:6185–6196, 2017.
- [10] E-H Essoufi and A Zafar. Boundary optimal control of time–space sir model with nonlinear robin boundary condition. *International Journal of Dynamics and Control*, 10(4):1279–1290, 2022.

- [11] O Elamraoui, E-H Essoufi, and A Zafrar. Spatio-temporal sir model with robin boundary condition and automatic lockdown policy. *International Journal of Applied and Computational Mathematics*, 9(1):1–18, 2023.
- [12] Linda JS Allen, Ben M Bolker, Yuan Lou, and Andrew L Nevai. Asymptotic profiles of the steady states for an sis epidemic reaction-diffusion model. *Discrete & Continuous Dynamical Systems*, 21(1):1, 2008.
- [13] E Bertuzzo, Renato Casagrandi, Marino Gatto, I Rodriguez-Iturbe, and A Rinaldo. On spatially explicit models of cholera epidemics. *Journal of the Royal Society Interface*, 7(43):321–333, 2010.
- [14] Robert Stephen Cantrell and Chris Cosner. *Spatial ecology via reaction-diffusion equations*. John Wiley & Sons, 2004.
- [15] Clare Menozzi. International migration 2020 highlights. 2021.
- [16] Fred Brauer and Pauline van den Driessche. Models for transmission of disease with immigration of infectives. *Mathematical Biosciences*, 171(2):143–154, 2001.
- [17] Xinxin Wang, Shengqiang Liu, Lin Wang, and Weiwei Zhang. An epidemic patchy model with entry–exit screening. *Bulletin of mathematical biology*, 77(7):1237–1255, 2015.
- [18] C Connell McCluskey and P van den Driessche. Global analysis of two tuberculosis models. *Journal of Dynamics and Differential Equations*, 16(1):139–166, 2004.
- [19] Ram P Sigdel and C Connell McCluskey. Global stability for an sei model of infectious disease with immigration. *Applied Mathematics and Computation*, 243:684–689, 2014.
- [20] Ram P Sigdel and C Connell McCluskey. Disease dynamics for the hometown of migrant workers. *Mathematical Biosciences & Engineering*, 11(5):1175, 2014.
- [21] Huashui Zhan. Reaction diffusion equations with boundary degeneracy. 2016.
- [22] MS Floater. Blow-up at the boundary for degenerate semilinear parabolic equations. *Archive for Rational Mechanics and Analysis*, 114(1):57–77, 1991.
- [23] Yongbin Ge, Zhiquan Cai, and Qin Sheng. A compact adaptive approach for degenerate singular reaction-diffusion equations. *Numerical Methods for Partial Differential Equations*, 34(4):1166–1187, 2018.

- [24] Amit Einav, Jeffrey J Morgan, and Bao Q Tang. Indirect diffusion effect in degenerate reaction-diffusion systems. *SIAM Journal on Mathematical Analysis*, 52(5):4314–4361, 2020.
- [25] O Elamraoui, EH Essoufi, H Rahnaoui, and A Zafrar. A time-space sir model for disease spread across two regions: Analysis and numerical simulations. *International Journal of Biomathematics*, 18(05):2450006, 2025.
- [26] Nicolas Privault. *Spatial Poisson Processes*, pages 225–239. Springer Singapore, Singapore, 2013.
- [27] C. Wang. Approximate controllability of a class of semilinear systems with boundary degeneracy. *Journal of Evolution Equations*, 10(1):163–193, 2010.
- [28] F. D. Araruna, B. S. V. Araújo, and E. Fernández-Cara. Carleman estimates for some two-dimensional degenerate parabolic pdes and applications. *SIAM Journal on Control and Optimization*, 57(6):3985–4010, 2019.
- [29] W. Wu, Y. Hu, Y. Liu, and D. Yang. Carleman estimates for degenerate parabolic equations with single interior degeneracy point and applications. *Mathematical Control and Related Fields*, 2025.
- [30] Roger Temam. *Navier–Stokes equations: theory and numerical analysis*, volume 343. American Mathematical Society, 2024.